



Published in final edited form as:

*J Occup Environ Hyg.* 2015 ; 12(4): 245–255. doi:10.1080/15459624.2014.970273.

## An Empirical Model of Human Aspiration in Low-Velocity Air Using CFD Investigations

T. Renée Anthony<sup>a</sup> and Kimberly R. Anderson<sup>b</sup>

<sup>a</sup>Department of Occupational and Environmental Health, University of Iowa, Iowa City, Iowa

<sup>b</sup>Department of Environmental and Radiological Health, Colorado State University, Fort Collins, Colorado

### Abstract

Computational fluid dynamics (CFD) modeling was performed to investigate the aspiration efficiency of the human head in low velocities to examine whether the current inhaled particulate mass (IPM) sampling criterion matches the aspiration efficiency of an inhaling human in airflows common to worker exposures. Data from both mouth and nose inhalation, averaged to assess omnidirectional aspiration efficiencies, were compiled and used to generate a unifying model to relate particle size to aspiration efficiency of the human head. Multiple linear regression was used to generate an empirical model to estimate human aspiration efficiency and included particle size as well as breathing and freestream velocities as dependent variables. A new set of simulated mouth and nose breathing aspiration efficiencies was generated and used to test the fit of empirical models. Further, empirical relationships between test conditions and CFD estimates of aspiration were compared to experimental data from mannequin studies, including both calm-air and ultra-low velocity experiments. While a linear relationship between particle size and aspiration is reported in calm air studies, the CFD simulations identified a more reasonable fit using the square of particle aerodynamic diameter, which better addressed the shape of the efficiency curve's decline toward zero for large particles. The ultimate goal of this work was to develop an empirical model that incorporates real-world variations in critical factors associated with particle aspiration to inform low-velocity modifications to the inhalable particle sampling criterion.

### Keywords

dust sampling convention; human aspiration; inhalability; inhalable dust; low velocity; model

### INTRODUCTION

To assess the risk of exposure to inhaled particles that are detrimental to worker health, it is important to measure exposures in a way that represents how particles enter into and behave in the respiratory system. For particles that can cause health effects if deposited anywhere in the respiratory system, hygienists should measure dust concentrations with samplers that meet the sampling criterion presented in the inhalable particulate mass (IPM) efficiency curve.<sup>(1)</sup> The IPM curve was developed from experimental wind tunnel studies<sup>(2–5)</sup> by identifying the collection efficiency of a human mannequin's mouth and nose. These studies computed the aspiration efficiency fraction as the ratio of inhaled dust concentration to the

upstream challenge concentration. Samplers that meet the performance criterion of the IPM curve are intended to collect samples with an efficiency matching that of the human head, providing estimates of particle concentrations that represent what the workers inhale into their mouths/noses. This criterion has been established by the American Conference of Governmental Industrial Hygienists (ACGIH®), and adopted globally as:

$$I P M = 0.5 \left( 1 + e^{-0.06d_{ae}} \right) \quad (1)$$

where  $d_{ae}$  is the aerodynamic diameter (1–100  $\mu\text{m}$ ) of a particle being sampled.<sup>(1)</sup> Samplers that meet this criterion require small particles to be collected close to 100% efficiency, but particles exceeding 54  $\mu\text{m}$  are to be collected with only 50% efficiency, reflective of the efficiency in which particles of different sizes are aspirated into the human mouth and nose.

The initial studies<sup>(2–5)</sup> that formed the basis for the IPM criterion used wind tunnel studies where air velocities surrounding the human mannequins were much larger (1 to 9  $\text{m s}^{-1}$ ) than what currently exist in occupational settings (geometric mean 0.06  $\text{m s}^{-1}$ , 85% < 0.3  $\text{m s}^{-1}$ ).<sup>(6)</sup> Studies examining the effects of high wind speed on human inhalation<sup>(7)</sup> identified an increase in inhalability for large particles (70 to 100  $\mu\text{m}$ ), but in light of the 1998 workplace velocity studies<sup>(6)</sup> international activities have been undertaken to examine whether human aspiration might also differ from the IPM curve in low velocities.<sup>(8–12)</sup> Wind tunnel studies examining aspiration efficiency were conducted in low velocities to examine this hypothesis. Initial calm air chamber studies, including Hsu and Swift<sup>(8)</sup> and Aitken et al.<sup>(9)</sup> reported conflicting trends, with the former reporting aspiration efficiency approaching zero for 80  $\mu\text{m}$  particles while the latter identified aspiration exceeding the IPM criterion.

In recent years, low-velocity wind tunnel studies have examined aspiration efficiencies using mannequins. Kennedy and Hinds<sup>(10)</sup> examined aspiration at a wind speed of 0.4  $\text{m s}^{-1}$  and Sleeth and Vincent<sup>(11,12)</sup> examined aspiration at wind speeds ranging from 0.1 to 0.4  $\text{m s}^{-1}$ , both using full-size mannequins truncated at hip height, with mannequin rotation to assess aspiration across all orientations relative to the oncoming air. In wind tunnel studies, aspiration calculations require uniform particle distribution in both time and space. As the wind tunnel velocities decrease, this uniform particle distribution becomes more problematic: gravitational settling of particles begins to dominate the particle transport. For example, the terminal settling velocity of a 100  $\mu\text{m}$  particle is 0.3  $\text{m s}^{-1}$ , which exceeds the horizontal convective transport in ultra-low-velocity conditions (e.g., 0.1  $\text{m s}^{-1}$ ). Sleeth and Vincent<sup>(11)</sup> developed a dual distribution system for introducing particles both upstream of the mannequin (for small particles) and above the mannequin (for larger particles). Aspiration efficiency for mannequins was computed using the ratio of particle concentration entering the mouth/nose divided by the concentration upstream of the mannequin as measured from isokinetic samplers. Uncertainty in reference concentrations from isokinetic samplers in slow moving air, particularly with large particles, and ensuring wall deposits are adequately quantified are a continued concern in low-velocity wind tunnels.<sup>(13)</sup> Methods such as wiping reference samplers compared to rinsing their surfaces might under-extract deposited particles in these samplers, thereby underestimating upstream dust concentrations and overestimating computed aspiration efficiency.

To avoid the difficulties in obtaining and quantifying uniform upstream concentrations in wind tunnel experiments, studies relying on computational fluid dynamics (CFD) simulations have been underway to investigate human aspiration in slow moving air. To date, two research groups have investigated particle aspiration by the human head (mouth, nose) by examining fluid flow and particle transport into simulated human forms (“humanoids”) in slow-moving air. King Se et al.<sup>(14)</sup> have examined transport into both the mouth and nose of a male-dimensioned form that faces the wind. Concurrently, CFD studies examining multiple factors associated with aspiration into the mouth and nose have relied on a female-dimensioned form at multiple orientations relative to the wind.<sup>(15–20)</sup> Table I summarizes briefly the studies performed in this research group. Simulated wind tunnel velocities ranged from 0.1 to 0.4 m s<sup>-1</sup> and continuous suction through the mouth or nose used velocities selected to match the mean inhalation velocity from at-rest (7.5 L min<sup>-1</sup>) to heavy (50.3 L min<sup>-1</sup>) breathing rates.

These sets of aspiration estimates can be analyzed to provide a unified model for aspiration efficiency in low-velocity air, using CFD simulation estimates over the range of conditions studied: freestream velocities (0.1 to 0.4 m s<sup>-1</sup>), inhalation velocities (at-rest through heavy), breathing mode (mouth, nose), and facial features (small, large facial features). Data from omnidirectional simulations were used to allow comparison to mannequin studies, the current IPM criterion, and proposed low-velocity aspiration efficiency currently under consideration. This robust data set was used to develop and examine empirical relationships between CFD estimates of aspiration efficiency and particle size and other dependent variables pertinent to the field of aerosol dynamics. The resulting models were validated with an additional set of simulation data to select the most appropriate relationship between human aspiration and both particle size and significant environmental factors. The ultimate goal of this work is to provide an empirical model that incorporates multiple real-world variations in critical factors associated with particle aspiration (facial feature sizes, freestream velocity, breathing rate) to inform modifications to the inhalable particle sampling criterion for indoor air velocities.

## METHODS

### Simulations

Detailed descriptions of the CFD simulations have been provided,<sup>(16–19)</sup> but highlights are given here. The new simulations used to obtain validation data were performed using the same geometry (small nose), equations, and solutions as the simulations used to develop the empirical model.

Ansys 13.0 (Ansys Inc., Lebanon, NH) was used to generate the geometries and meshes and to simulate fluid and particle flow. A truncated cylinder (hip height) with an anatomically detailed neck and head based on 50<sup>th</sup> percentile female dimensions was generated. Two models of facial features were examined: small nose with small lips (proportioned to match laser Doppler velocity measurements in Anthony, Flynn, and Eisner<sup>(20)</sup>) and large nose with large lips, both described in detail in Anthony.<sup>(16)</sup> This humanoid form was positioned in a wind tunnel, at a fixed orientation per simulation (0° = facing the wind, 15, 30, 60, 90, 135, 180° relative to the oncoming wind). Figure 1 illustrates the humanoid geometry in the

simulated wind tunnel. A paved meshing scheme, using triangular surface and tetrahedral volumetric elements, was used to discretize the domain. For a random selection of the geometries, a set of three sequentially refined meshes was generated for convergence studies. The most refined mesh was on the order of 3 million nodes, with 17 mm average node spacing in the domain and 0.48 mm node spacing near the mouth and nose.

Simulations were conducted using 64-bit processors. All simulations presented here used steady-state, incompressible, turbulent Navier-Stokes equations and were solved using standard k-epsilon turbulence models with full buoyancy effects. The SIMPLE algorithm, with second-order upwinding, was applied. Indoor conditions (temperature of 20°C, air density of 1.205 kg m<sup>-3</sup>, air viscosity of 1.83692 × 10<sup>-5</sup> kg m<sup>-1</sup>s<sup>-1</sup>) were simulated. Boundary conditions assigned flow through the inlet to the simulated wind tunnel (0.1, 0.2, 0.4 m s<sup>-1</sup> for empirical model development and 0.31 m s<sup>-1</sup> was randomly selected for the validation data set). Constant velocities were applied to the mouth or nostril inlets to represent the mean velocity associated with three volumetric breathing rates: 7.5 (at-rest), 18 (moderate), and 50.3 (heavy) L min<sup>-1</sup>. The validation data used a breathing rate of 40.2 L min<sup>-1</sup>, randomly selected within the range above. Between geometries, simulation settings were matched on volumetric flow rate, requiring small changes to suction velocities assigned to the mouth and nose inlet surfaces.

Table II details the specific velocities based on the geometry under study. The size of the mouth orifice did not change throughout the study, but the nostril opening area changed by nose size, with the larger nose protrusion requiring larger nostril openings to make realistic facial features. Walls were assigned the no-slip condition, and initial estimates of velocity were assigned to the entire remaining domain by applying the virtual wind tunnel inlet values. For all simulations, a turbulence intensity of 8% and a ratio of eddy to laminar viscosity of 10, typical of wind tunnel studies, were applied to the domain entrance as a boundary condition and were also applied throughout the domain as initial conditions to all unassigned nodes. Iterative solutions were stopped when global solution errors (GSEs) reached predetermined tolerances of 10<sup>-3</sup>, 10<sup>-4</sup>, and 10<sup>-5</sup> to assess iterative solution convergence using L2 error norms. Mesh independence was assessed on randomly selected conditions to ensure the three-mesh R<sub>2</sub> values were less than unity.<sup>(21)</sup> Fluid flow solutions from the most refined solution (10<sup>-5</sup> GSE) and meshes were used for all subsequent particle simulations.

Particle simulations were performed using the critical area method described by Anthony and Flynn,<sup>(15)</sup> where the position of upstream particles that traveled through the virtual wind tunnel and terminated inside the humanoid's mouth or nose were identified. To achieve the assumption of uniform distribution of particles upstream of the inhaling humanoid, particles were released with initial velocities equivalent to the freestream velocity at the release location plus the terminal settling velocity (in the downward direction). Particles were released at upstream coordinates, allowing the motion of the particles to include convection in the solved fluid flow stream along with gravitational settling. The release coordinates of particles whose paths terminated in the mouth or nose of the humanoid were identified. The upstream area that contained all particles that traveled through the virtual wind tunnel and terminated inside the mouth/nose was identified as the

critical area ( $A_{critical}$ ). The coordinates of the outer edges of this streamtube at the upstream release location were used to compute the size and identify the location of  $A_{critical}$ .

The position and coordinates of the critical areas for particles of unit density ( $1000 \text{ kg m}^{-3}$ ) and diameters ( $d_{ae}$ ) 7, 22, 52, 68, 82, 100, and  $116 \mu\text{m}$  were determined for each simulation. Note that the upstream area through which particles travel into the mouth/nose ( $A_{critical}$ ) is not necessarily the same as the upstream area that contains the air which travels into the mouth/nose, particularly for particles with significant settling velocity relative to the freestream. Thus, the aspiration efficiency of each simulation condition, by particle size, was computed using the equation<sup>(15)</sup>:

$$A = \frac{A_{critical} U_{critical}}{A_s U_s} \quad (2)$$

where  $U_{critical}$  is the upstream freestream velocity within the critical area,  $A_s$  is the opening area of the inhaling mouth or nose, and  $U_s$  is the mouth or nose suction velocity assigned to the given simulation.

Particle simulations were conducted for the humanoid at specific orientations relative to the main airflow path in the virtual wind tunnel, and orientation-averaged calculations were made for each velocity condition and particle size simulated by weighting the seven individual estimates by the orientation's average contribution to the full  $360^\circ$  rotation, namely:

$$A = \frac{1}{24} A_0 + \frac{1}{12} A_{15} + \frac{1}{8} A_{30} + \frac{1}{6} A_{60} + \frac{5}{24} A_{90} + \frac{1}{4} A_{135} + \frac{1}{8} A_{180} \quad (3)$$

where the subscripts refer to the orientation relative to the oncoming wind and the weighting factor represents the proportion of the complete rotation that the study angle covers, similar to the work of Tsai et al.<sup>(22)</sup> The resulting orientation-averaged aspiration efficiencies were compared to the current IPM sampling criterion<sup>(1)</sup> and the proposed low-velocity aspiration efficiency curves recommended by Aitken et al.<sup>(9)</sup>

## Empirical Model Development

For each breathing mode (mouth, nose), suction velocity (3, in Table II, matching mean inhalation velocity at volumetric breathing rates of  $7.5 = \text{at-rest}$ ,  $18 = \text{moderate}$ , and  $50.3 = \text{heavy L min}^{-1}$ ), and freestream velocity ( $0.1, 0.2, \text{ and } 0.4 \text{ m s}^{-1}$ ), omnidirectional averaged estimates of aspiration efficiency were computed for seven particle sizes identified earlier. Ninety-eight omnidirectional aspiration estimates were generated for the small nose/small lip, with an additional 14 estimates for the large nose/large lip geometry with nose breathing ( $0.4 \text{ m s}^{-1}$  freestream with at-rest breathing and  $0.1 \text{ m s}^{-1}$  at moderate breathing). Since the large facial features have been previously associated with small decreases (8%) in aspiration efficiency compared to smaller features, this work relied more heavily on simulations associated with the larger aspiration efficiencies, which would yield more conservative (larger) estimates for the broad range of facial features applicable to real workers. Fourteen estimates of aspiration were made for mouth and nose (small nose/small lip) at the validation test condition ( $0.31 \text{ m s}^{-1}$  freestream and  $40.2 \text{ L min}^{-1}$  equivalent breathing rate).

Plots were generated to identify general relationships between parameters prior to fitting empirical models to examine initial assumptions, such as the appropriateness of linear shape and whether simple trends in aspiration by freestream or suction velocity warranted examination of interaction.

The relationship between aspiration and the independent variables in CFD aspiration efficiency simulations was examined (multiple linear regression, PROC REG using SAS 9.3, SAS Institute, Raleigh, NC). All models used the aerodynamic diameter ( $d_{ae}$ ) for the particle size indicated, and regression models examined both fitting the intercept as well as forcing it to 1 at small particle diameters. Equation forms included a linear relationship between aspiration and particle size, such as that of Aitken et al.,<sup>(9)</sup> and a squared particle diameter, as the shape of the resulting aspiration fractions by particle size did not appear linear. Additional data transformations were included in this analysis to incorporate significant factors reported in earlier thin-walled sampler efficiency studies, including the ratio of suction velocity ( $U_s$ ) to freestream velocity ( $U_o$ ), specifically  $U_o / U_s$  as reported in blunt sampler theory by Vincent and Mark<sup>(4)</sup> and disk-shaped samplers of Ingham and Wen.<sup>(23)</sup> In addition, because the Stokes number (St) describes the ratio of the characteristic response time of a fluid to that of a particle, it was also included in this analysis. In low Reynolds number regimes, the Stokes number is computed by using:

$$St = d_p^2 \rho_p \pi U / (18 \mu D) \quad (4)$$

where  $d_p$  is the physical particle diameter,  $\rho_p$  is the particle density,  $\mu_g$  is the gas viscosity, and  $D$  is the characteristic dimension of the obstacle (here, the humanoid). Traditionally, the velocity term is assigned as the freestream velocity, significantly upstream of the obstacle (the humanoid), which is our modeled freestream velocity,  $U_o$ . Since our simulated aspiration efficiency used constant particle density ( $\rho_p$ ), ambient temperature and pressure, and torso/head diameter ( $D$ ), the examination of Stokes number could be simplified to ( $d_{ae}^2 \times U_o$ ) in regression modeling. Because suction velocity also affects particle motion in the region of the mouth and nose, an alternative Stokes number formulation was also examined independently from the traditional freestream velocity formulation, namely  $d_{ae}^2 \times U_s$ .

Regression models with single and multiple variables were generated to examine the factors that had the most statistically significant and relevant influence on the estimation of aspiration efficiency. An independent variable was determined to be significant at  $\alpha = 0.05$ ; for multi-term models, backwards elimination was used. Over all simulation conditions, the significant independent variables were then evaluated to determine the relative contribution of each factor's influence on estimates of aspiration efficiency in attempts to find a unifying model for low-velocity aspiration. Aspiration efficiency residuals were computed by subtracting the CFD-simulated estimate from the estimate computed from using the empirical model. Residuals were assessed qualitatively by plotting to ensure random pattern to residuals over independent factors and quantitatively by identifying the model with the lowest standard deviation of residuals. Finally, the empirical models' estimated aspiration efficiencies were compared to the CFD efficiency estimates, both with the data used to generate the empirical model and independently with the new validation data set ( $0.31 \text{ m s}^{-1}$  freestream velocity), to examine which empirical model performed better in estimating

aspiration efficiency for the new validation condition. Aspiration data from experimental ultra-low-velocity mannequin studies<sup>(11)</sup> were also compared to the resulting empirical models.

## RESULTS

Fluid simulations for the 14 new geometry-orientation validation data required approximately 10 days of simulation time, per condition (140 computer-days) using 12 GB Ram computers. Table III contains aspiration efficiency results for the new simulation conditions used to validate the empirical models. Figure 2 contains all simulated aspiration efficiencies used to generate the empirical model, reported in full previously.<sup>(18,19)</sup> As has been reported, the aspiration efficiency of the human head decreased with increasing particle size, with few larger particles capable of turning into the inhaling mouth or nose relative to smaller particles. In this low-velocity regime, aspiration efficiency increased with decreasing freestream velocity, and the difference in estimates increased with increasing particle diameter, supporting examination of the interaction of  $d_{ae}$  and  $U_o$  in the regression models. Heavy breathing simulations yielded larger estimates of aspiration efficiency, a trend consistent across all freestream velocities and breathing mode. Matched by freestream and equivalent volumetric suction, inhalation through the nose resulted in smaller aspiration efficiencies than mouth inhalation across all conditions tested. Figure 3 overlays both the IPM sampling criterion and the three Aitken et al.<sup>(9)</sup> curves with the aspiration efficiencies for at-rest and moderate breathing simulations. (Note that our “heavy” simulations with suction velocities at an equivalent cyclical breathing rate in the range of  $50 \text{ L min}^{-1}$  were outside of the range of Aitken et al.’s<sup>(9)</sup> experiments and are therefore not shown.)

Because of these trends, examination of fitting a unified model for aspiration efficiency included examining the relationship between aspiration fraction and particle size, combined with freestream velocity and suction velocity as well as the velocity ratio ( $U_o / U_s$ ), the interactions of particle size with suction velocity ( $d_{ae} \times U_s$ ) and with freestream velocity ( $d_{ae} \times U_o$ ). Table IV illustrates the best-fitting relationships between aspiration and factors evaluated in this study. Equations include all significant independent variables at  $\alpha = 0.05$ ; the p-values for the model ANOVA F-test were all  $< 0.0001$ . Plots of residuals confirmed random distribution over each independent factor used in each model. Information on the range of residuals for each model along with a standard deviation of those residuals, is presented in Table V.

### Regression on $d_{ae}$

Relying on only particle diameter, the least squared regression with forced intercept of 1 yielded  $A = 1 - 0.00785d_{ae}$  (ID 1 in Table IV). To obtain equations in the form of Aitken et al.,<sup>(9)</sup> namely  $A = 1 - Kd_{ae}$ , simple linear regression by breathing rate, with forced intercept of 1 for small particles, identified the following  $K$  terms: At-rest ( $7.5 \text{ L min}^{-1}$ ) = 0.0092, Moderate ( $20.8 \text{ L min}^{-1}$ ) 0.0077, Heavy ( $50.3 \text{ L min}^{-1}$ ) = 0.0054. Aitken et al.<sup>(9)</sup> reported  $K$  values of 0.0076 to 0.0038 for 6 to  $20 \text{ L min}^{-1}$  breathing rates, respectively. While the  $K$  terms from this CFD simulation and Aitken’s calm air studies differed slightly, they were

the same order of magnitude and resulted in the same trending with decreasing aspiration efficiency with increased suction velocity.

Equation ID 2 includes a breathing rate term with particle size in a single linear relationship for aspiration, with modest improvement in the  $R^2$ . Additional linear models combining particle size and velocity terms are given in Table IV in ID 3 through 5, with the most complete model yielding the best coefficient of determination ( $R^2 = 0.91$ ). By including both velocities, all terms ( $d_{ae}$ ,  $U_s$ ,  $U_o$ ) were significant, improving the predictive model by 10% over the simple one-term model in ID 1. However, in plotting each linear relationship between aspiration and particle size, the trend of overestimating aspiration for small particles and underestimating for large particles at heavy and moderate breathing is clear (Figure 4). The overall range of residuals was minimized from  $-0.38/+0.39$  to  $-0.22/+0.26$  (standard deviation 0.14 to 0.10) by including suction and freestream velocity as well as particle size as a factor for aspiration estimation (Table V).

### Regression on $d_{ae}^2$

To accommodate the shape of the relationship between aspiration and particle size, empirical models using diameter squared were explored (ID 6 through 8 in Table IV). Including particle diameter with its squared term improved the fit, and both velocities were significant contributors ( $p < 0.005$ ) to the regression model. The Stokes term ( $d_{ae}^2 \times U_o$ ) was significant only if it replaced the particle diameter squared term in the model (ID 10); this variable rendered the  $d_{ae}^2$  term insignificant ( $p = 0.40$ ), as one might expect. Further, if the freestream velocity ( $U_o$ ) was used directly in the model, the Stokes term then became insignificant ( $p = 0.18$ ). Other interactions were explored based on the trends in data between aspiration and velocity (ID 11 through 13). In comparing ID 10 to ID 11, using  $d_{ae}^2$  yielded improved  $R^2$  over the Stokes term, and this simpler form was moved forward in the analysis.

The equation presented as ID 13 is the most complex model for which all factors are significant. The signs of the factors are appropriate for the trends identified in the data. The interaction of particle size and suction velocity has a positive coefficient, and when both particle size and suction increase, aspiration determined by the CFD simulations did increase. The coefficient for the velocity ratio was negative, consistent with both trends of (1) decreased aspiration fraction with increased freestream velocity at steady breathing rate, and (2) increased aspiration with increased suction velocity, holding freestream steady. The resulting model from ID 13 was plotted in Figure 5 to illustrate how the shape of the second-order model improved over the linear expressions (Figure 4), where the alternate Stokes formulation, using suction velocity instead of the freestream velocity, and the velocity ratio were used. While simulation data for the condition with the largest aspiration efficiencies ( $0.1 \text{ m s}^{-1}$  at heavy breathing, mouth) and the lowest aspiration efficiencies ( $0.4 \text{ m s}^{-1}$  at rest breathing, nose) were just outside the regression plots, the general shape and agreement with data trends are improved over the linear models.

The range of residuals was unchanged by including  $d_{ae}^2$  along with all single-term factors (ID 8 compared to ID 5, Table V). However, by including the velocity ratio ( $U_o/U_s$ ), the residuals were reduced ( $-0.35/+0.48$  for ID 8 to  $-0.21/+0.28$  for ID 11). Over the entire

range of empirically modeled aspiration estimations, the standard deviation of residuals was minimized (0.08) with the most complicated model (ID 13), with models ID 11 and ID 8 performing nearly as well over the range of particle sizes and flow rates examined, which is obviously consistent with the  $R^2$  statistic.

### Comparison to New Simulated and Experimental Aspiration Efficiency

Figure 6 plots the new experimental CFD simulation estimates (“cfd-new,” square data markers,  $N = 14$ ) versus aspiration estimated from two empirical models: the best-fitting linear model (ID 5) and the most comprehensive model with particle diameter squared (ID 13). The regression between the CFD simulation estimates and modeled estimates of aspiration efficiency had similar goodness of fit ( $R^2 = 0.91$  for linear, 0.94 for  $d_{ac}^2$  models). The agreement between CFD aspiration and empirically estimated aspiration from the ID 5 model yielded a good  $R^2$  (0.94). However, the relationship between CFD-generated aspiration and empirically estimated aspiration differed from that in the relationship used to generate the model (data plotted as “cfd-original,” diamond markers) by 16% in slope (from 0.89 to 1.04) for the new condition and the model-generating aspiration estimates. For the ID 13 model, the  $R^2$  remained good with the new CFD data (0.97), and the slopes relating CFD-generated aspiration and empirically modeled aspiration differed by only 3% (0.93 to 0.90) for the new CFD aspiration estimate data compared to the data used to generate the empirical model. However, the intercept shifted with the new CFD data-empirical estimate relationship, associated with an aspiration fraction shift of 0.09 (Figure 6b).

Comparisons to Sleeth and Vincent<sup>(12)</sup> wind tunnel data (Figure 6, round markers) found the same trends in aspiration by freestream velocity, namely that slower freestream yielded larger aspiration in the range of 0.1 to 0.4  $m\ s^{-1}$ . However, data variability in aspiration calculations yielded uncertain trends in the importance of breathing rate on aspiration, over the range of 6 to 20  $L\ min^{-1}$  cyclical breathing. In fitting their mean aspiration measurements to the empirical models ID 5 and ID 13 (Figure 6), the scatter in the Sleeth and Vincent data reduced the fit to  $R^2 = 0.51$  and 0.45, respectively, with nearly equivalent slope and intercept agreement for both the linear and the more complex  $d_{ac}^2$  model.

## DISCUSSION

Estimating aspiration efficiency using CFD was useful to avoid potential biases existing in wind tunnel studies. Wind tunnel experiments require delivering and accurately quantifying uniform particle concentrations upstream of an inhaling mannequin. Particles larger than 57  $\mu m$  have gravitational settling velocities on the order of low-flow indoor air velocities (0.1 to 0.3  $m\ s^{-1}$ ), which contribute to vertical motion as well as horizontal motion toward an inhaling mannequin. Maintaining a concentration that is spatially and temporally uniform across the entire wind tunnel cross-section is difficult.<sup>(24)</sup> Since quantified upstream concentrations, using isokinetic samplers often positioned at mouth height but to the side or upstream of an experimental mannequin, are used as the denominator in aspiration calculations, uncertainties in these measures contributes greatly to uncertainty in wind tunnel aspiration estimates. CFD can allow the modeler to explicitly generate uniform upstream concentrations and to specify operation parameters that may change over time

during wind tunnel experiments (e.g., freestream velocities and breathing rates): controlling these factors reduces these uncertainties when simulating particle transport. The methods used to quantify CFD aspiration estimates resulted in uncertainties on the order of 1%, mostly attributable to particle injection release position refinement.

However, this work did not inherently include turbulent particle transport, which introduces variability into the paths particles travel through the airflow when approaching the humanoid. Instead, the particle simulations here relied on laminar particle trajectory analysis to identify the upstream critical areas, within which all particles terminated inside the mouth or nose of the inhaling humanoid. While this provided an efficient method to identify the mean critical area, additional uncertainty of human aspiration by the factors studied here would require the use of turbulent particle simulations, with the random walk feature assigned to each step of the particle's transport and numerous repeated particle simulations. While preliminary work on this effect is not reported here, these simulations for one set of geometry and velocity simulations required approximately 14 days and 12 computers (168 computer-days) to obtain stable aspiration efficiency estimates per particle size. For just the new validation test conditions in this study, an estimated 16,000 computer-days would be needed to fully explore the turbulent particle trajectory method. While computer simulation speeds and memory allocation have improved over the duration of this research, the scope of the computational work to fully explore the test conditions studied here remains untenable without supercomputing.

To achieve CFD simulations in a reasonable amount of time, the simulations necessarily require abstractions from reality. While a realistic head/neck was modeled, the torso was simplified into a simple geometry to improve simulation times: the effect of this simplification is negligible based on findings of earlier work indicating that while the torso shape affects the position of the critical area, it did not affect the resulting estimates of aspiration efficiency.<sup>(17)</sup> The time-dependent nature of breathing was simplified to continuous inhalation, reducing the simulation time to 10 days per combination of geometry and velocity settings: cyclical breathing would have required time-dependent simulations of airflow and particles which would have added to the complexity of the model and simulation time. The effect of this simplification has not been directly evaluated, but expired air is known to disrupt the airflow upstream of study mannequins<sup>(24)</sup> which likely disturbs the upstream concentration of aerosols, rendering the immediate area upstream of the mouth/nose no longer uniform. While the stepwise investigation of the effect of orientation relative to the main path of freestream air also ignored the impact of human motion on the aspiration phenomenon, it has allowed a greater understanding of the reduced aspiration efficiency of the human head as the human form is rotated away from facing the wind.<sup>(18,19)</sup> Finally, this work relied on constant temperature, thereby ignoring thermal heating from the body positioned in room temperature air at low velocity: this simplification was presumed to have limited bias on the CFD model based on findings of Schmees et al.,<sup>(24)</sup> who indicated that the airflow induced by this thermal gradient had no appreciable effect on the airflow pattern in the breathing zone of a heated mannequin.

This study included an analysis of the form of the relationship between aspiration efficiency and particles size: linear versus squared aerodynamic diameter. The theoretical basis for

examining particle size squared includes the consideration of the Stokes number to incorporate response time. In more practical terms, as is shown in the differences between Figures 4 and 5, the shape of the data better fit the squared relationship in the CFD simulation data: we identified a sharp decrease in aspiration efficiency with increased particle size which is difficult to explain using linear relationship between particle size and aspiration efficiency.

One key difference between CFD simulations and wind tunnel experiments was identified: simulations identified that there is some limit to the aspiration of large particles in slow moving air, whereas the majority of wind tunnel experiments have not. The one exception are the Hsu and Swift<sup>(8)</sup> calm air studies, which identified a cutoff at  $\sim 80 \mu\text{m}$ . CFD simulations identified that as particle size increases toward  $100 \mu\text{m}$ , large particles cannot easily overcome the gravitational settling in slow moving air and aspiration approaches zero, particularly with low inhalation velocities. Wind tunnel studies typically report large uncertainty in aspiration estimates with increased particle size, and low freestream velocity aspiration tests of particles larger than  $70 \mu\text{m}$  are limited. Aspiration efficiency for wind tunnel tests at low velocities<sup>(12)</sup> report the lowest aspiration of 0.33 for  $63 \mu\text{m}$  ( $0.42 \text{ m s}^{-1}$  freestream at  $6 \text{ L min}^{-1}$  cyclical breathing), similar to the 0.33 identified for  $68 \mu\text{m}$  particles at  $0.4 \text{ m s}^{-1}$  and at-rest breathing in simulation work. It is unclear whether the wind tunnel data would identify linear decrease in aspiration as particle size increased above this size or whether the shape has a faster rate of decline, as indicated in the CFD simulations. These CFD simulation studies support the premise that an “upper bound” exists for human aspiration. As particle size increases, the effect of gravitational settling dominates particle motion and large particles, uniformly suspended, cannot transport into the human mouth or nose. As such, reliance on the IPM sampling curve that requires a 50% sampling efficiency for ultra-large inhalable particles ( $>80 \mu\text{m}$ ) may be inappropriate for slow moving air.

The dependence of aspiration on freestream velocity is likely similar for both human and sampler aspiration: as the velocity around a person changes, the same change to aspiration for a sampler and the human may likely occur. However, the dependence of human aspiration on breathing rate poses a problem to the ultimate development of a single sampling criterion: breathing rate changes with worker task and other personal factors, but a sampler typically operates at a constant flow rate. Knowing which suction velocity to match becomes important. As a practical matter, recommending a sampling criterion to match that of a moderate or moderate-to-high breathing rate would lead to decisions that are more protective of worker health, where a sample would yield a higher concentration than was actually inhaled for a worker with a slower breathing rate. However, health effects studies relying on these samplers that may over-aspirate particles should consider inclusion of work activity, thereby breathing rate, in exposure outcome studies.

## CONCLUSION

This work identified several factors, in addition to particle size, that are critical to estimating human aspiration efficiency of particles in slow moving air. Freestream velocity and breathing velocity (or rate) are useful for estimating aspiration efficiency, but an empirical model relying on these factors with a first-order particle aerodynamic diameter term

overestimates aspiration for small particles and underestimates for large particles at heavy and moderate breathing. Using a second-order particle diameter term ( $d_{ae}^2$ ) agrees better with the shape of the aspiration data, where CFD simulations identify an upper limit to particle aspiration, particularly in slow breathing. A full model that incorporates  $d_{ae}^2$ , the interaction of particle size, and suction velocity, and the ratio of freestream to suction velocity, provides a complete model that captures the change of aspiration efficiency over the range of conditions present in workplace environments:  $A = 1.01 - 3.58E-5 d_{ae}^2 - 0.005 d_{ae} + 2.5E-4 (d_{ae} \times U_s) - 0.79 (U_o/U_s)$ .

## ACKNOWLEDGMENTS

Thanks to the many involved in simulation work to generate data for this manuscript, including: Alysha Meyers, Jacob Krzystowczyk, Kelsie Reeve, Brian Pavlonis, Bela Huang, and Benjamin Getschman. Thanks to Dr. Darrah Sleeth for access to aspiration data for inhaling mannequin studies in low-velocity wind tunnels.

### FUNDING

This work was funded by the National Institute for Occupational Safety and Health, Centers for Disease Control (R01 OH009290). The contents are solely the responsibility of the authors and do not necessarily represent the official views of NIOSH.

## References

1. American Conference of Governmental Industrial Hygienists (ACGIH®). Threshold Limit Values for Chemical Substances and Physical Agents and Biological Exposure Indices. ACGIH; Cincinnati, OH: 2014.
2. Ogden TL, Birkett JL. The human head as a dust sampler. *Inhaled Particles*. 1975; 4:93–105. [PubMed: 1236176]
3. Vincent JH, Armbruster L. On the quantitative definition of the inhalability of airborne dust. *Ann. Occup. Hyg.* 1981; 24(2):245–248. [PubMed: 7316326]
4. Armbruster L, Breuer H. Investigations into defining inhalable dust. *Ann. Occup. Hyg.* 1982; 26(1): 21–32. [PubMed: 7181266]
5. Vincent JH, Mark D. Applications of blunt sampler theory to the definition and measurement of inhalable dust. *Ann. Occup. Hyg.* 1982; 26(1):3–19. [PubMed: 7181272]
6. Baldwin PE, Maynard AD. A survey of wind speeds in indoor workplaces. *Ann. Occup. Hyg.* 1998; 42(5):303–313. [PubMed: 9729918]
7. Vincent JH, Mark D, Miller BG. Aerosol inhalability at higher wind speeds. *J. Aerosol Sci.* 1990; 21(4):577–586.
8. Hsu DJ, Swift DL. The *in vitro* measurements of human inhalability of ultra-large aerosols in calm air conditions. *J. Aerosol Sci.* 1999; 30:1331–1343.
9. Aitken RJ, Baldwin PEJ, Beaumont BC. Aerosol inhalability in low air movement environments. *J. Aerosol Sci.* 1999; 30:613–626.
10. Kennedy NJ, Hinds WC. Inhalability of large solid particles. *J. Aerosol Sci.* 2002; 33:237–255.
11. Sleeth DK, Vincent JH. Inhalability for aerosols at ultra-low wind speeds. *J. Physics: Conf. Series*. 2009; 151:012062.
12. Sleeth DK, Vincent JH. Proposed modification to the inhalable aerosol convention applicable to realistic workplace wind speeds. *Ann. Occup. Hyg.* 2011; 55(5):476–484. [PubMed: 21257744]
13. Haddow, B.; Sleeth, DK. Comparison of methods to quantify wall losses in isokinetic samplers. 2014.
14. King, Se; M., C.; Inthavong, K.; Tu, J. Inhalability of micron particles through the nose and mouth. *Inhal. Toxicol.* 2010; 22:287–300. [PubMed: 20070173]
15. Anthony TR, Flynn MR. Computational fluid dynamics investigation of particle inhalability. *J. Aerosol Sci.* 2006; 37(6):750–765.

16. Anthony TR. Contribution of facial feature dimensions and velocity parameters on particle inhalability. *Ann. Occup. Hyg.* 2010; 54(7):710–725. [PubMed: 20457783]
17. Anderson KR, Anthony TR. Uncertainty in aspiration efficiency estimates due to torso simplifications in computational fluid dynamics (CFD) simulations. *Ann. Occup. Hyg.* 2013; 57(2):184–199. [PubMed: 23006817]
18. Anthony TR, Anderson KR. Computational fluid dynamics investigation of human aspiration in low velocity air: Orientation effects on mouth breathing simulations. *Ann. Occup. Hyg.* 2013; 57(6):740–757. [PubMed: 23316076]
19. Anderson KR, Anthony TR. Computational fluid dynamics investigation of human aspiration in low velocity air: Orientation effects on nose breathing simulations. *Ann. Occup. Hyg.* 2014; 58(5): 625–645. [PubMed: 24665111]
20. Anthony TR, Flynn MR, Eisner A. Evaluation of facial features on particle inhalation. *Ann. Occup. Hyg.* 2005; 49(2):179–193. [PubMed: 15734830]
21. Stern F, Wilson RV, Coleman HW. Comprehensive approach to verification and validation of CFD simulations—Part 1: Methodology and procedures. *J. Fluids Eng.* 2001; 123:793–802.
22. Tsai P-J, Vincent JH, Mark D. Impaction models for the aspiration efficiencies of aerosol samplers in moving air under orientation-averaged conditions. *Aerosol Sci. Technol.* 1995; 22:271–286.
23. Ingham DB, Wen X. Disk-like body sampling in a turbulent wind. *J. Aerosol Sci.* 1993; 24(5):629–642.
24. Schmees DK, Wu Y-H, Vincent JH. Visualization of the airflow around a life-sized, heated, breathing mannequin at ultra-low wind speeds. *Ann. Occup. Hyg.* 2008; 52(5):351–360. [PubMed: 18497432]

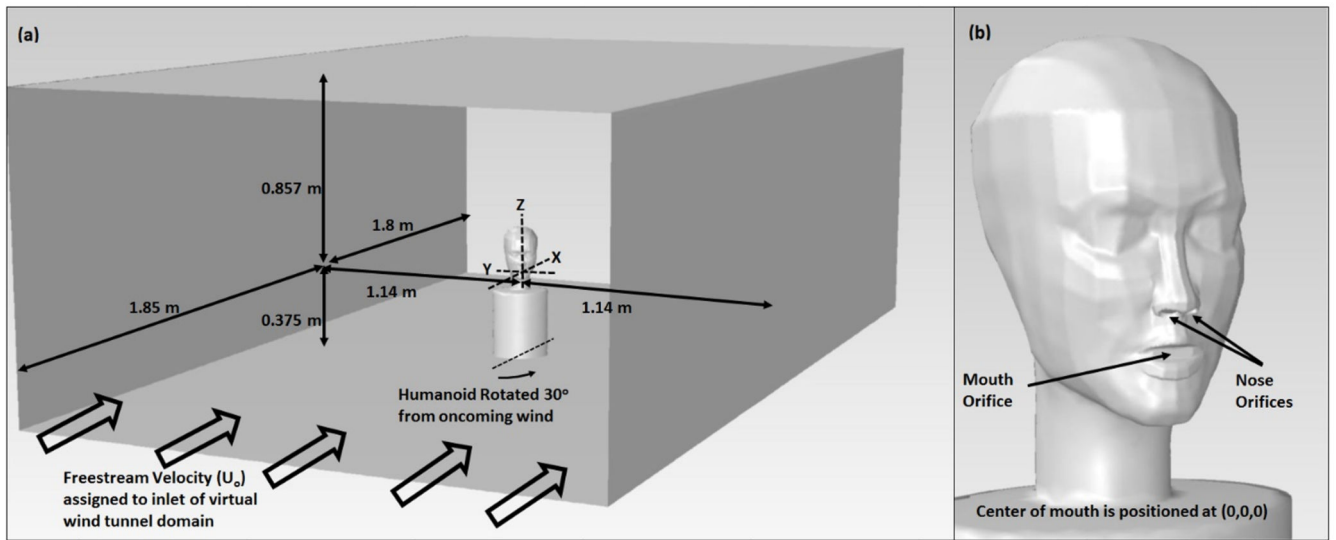


**FIGURE 1.** Example geometry illustrating dimensions and orientation for (a) entire domain with humanoid rotated 30° and (b) close-up of head illustrating mouth and nose inhalation orifices (small nose- small lip head geometry)

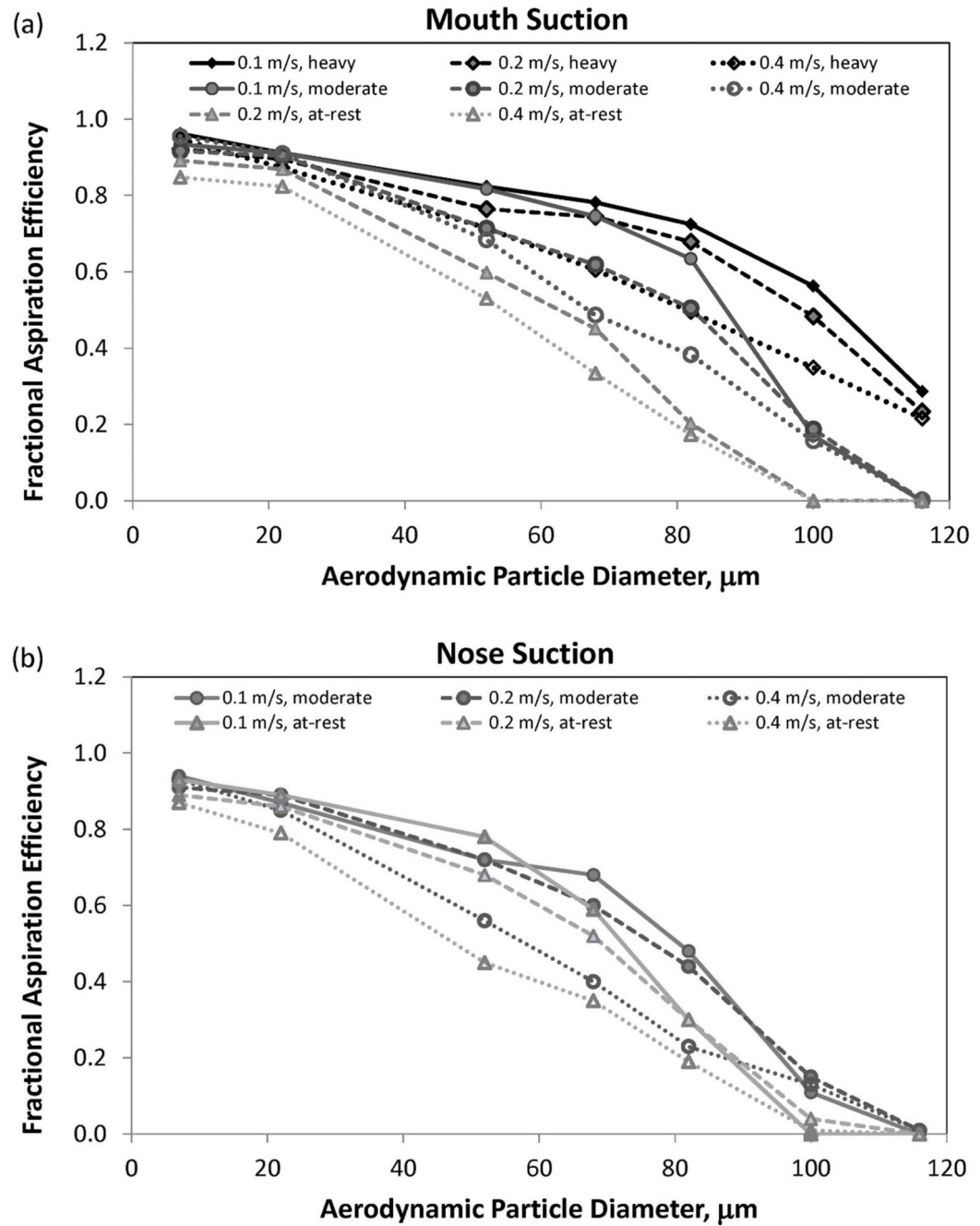


**FIGURE 2.** Aspiration versus particle aerodynamic diameter, for (a) mouth and (b) nose breathing simulations. The legend indicates freestream velocity, breathing rate.

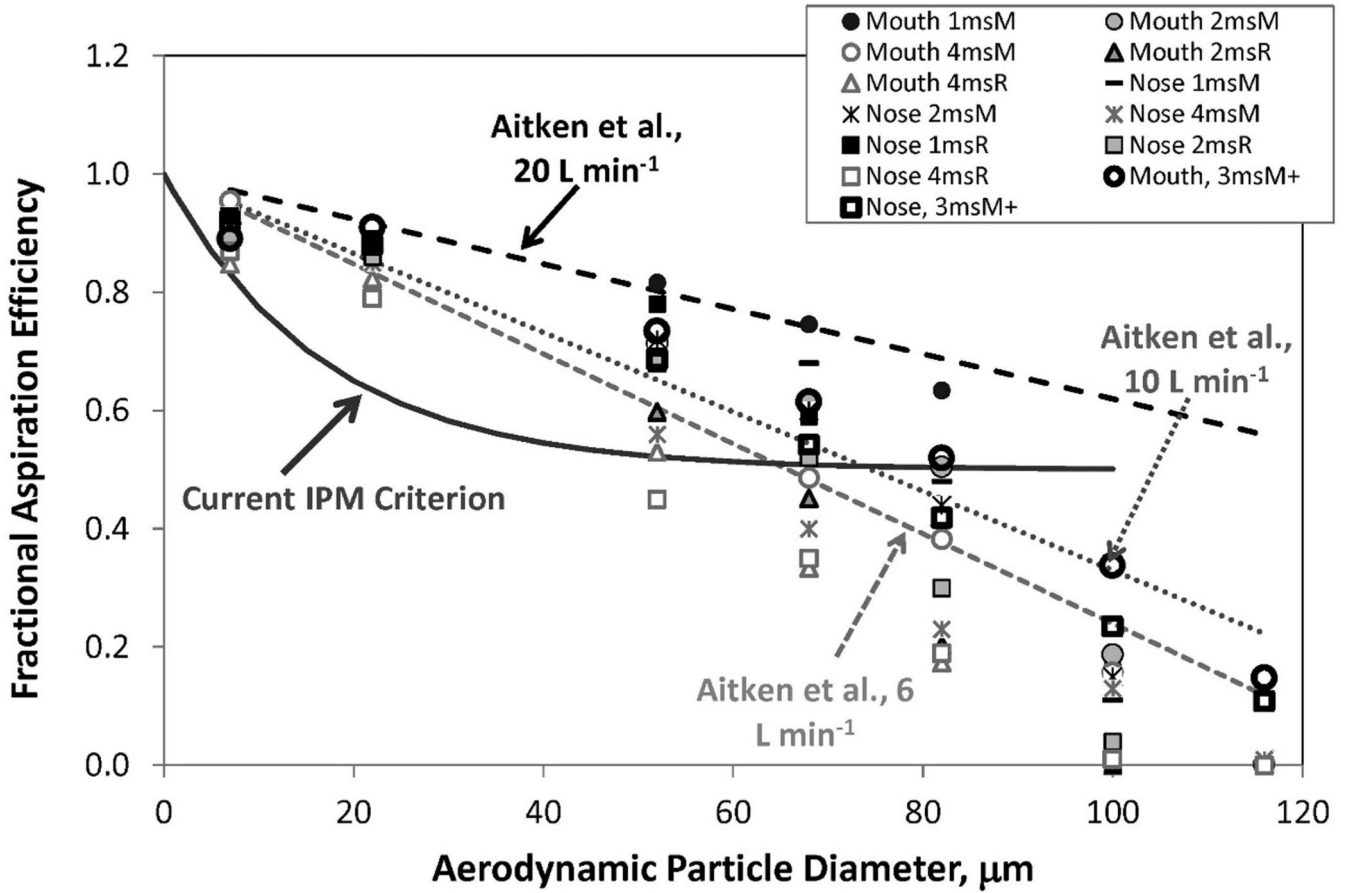


**FIGURE 3.** Simulated aspiration efficiency data for at-rest (R, 7.5 L min<sup>-1</sup> equivalent) and moderate (M, 18 L min<sup>-1</sup>) and the validation data (3msM+, with 0.3 m s<sup>-1</sup> freestream velocity and 40.2 L min<sup>-1</sup> equivalent breathing rate) compared to the current IPM curve (solid) and Aitken et al.<sup>(9)</sup> calm air aspiration efficiency equations (dashed lines) at the three breathing rates reported.

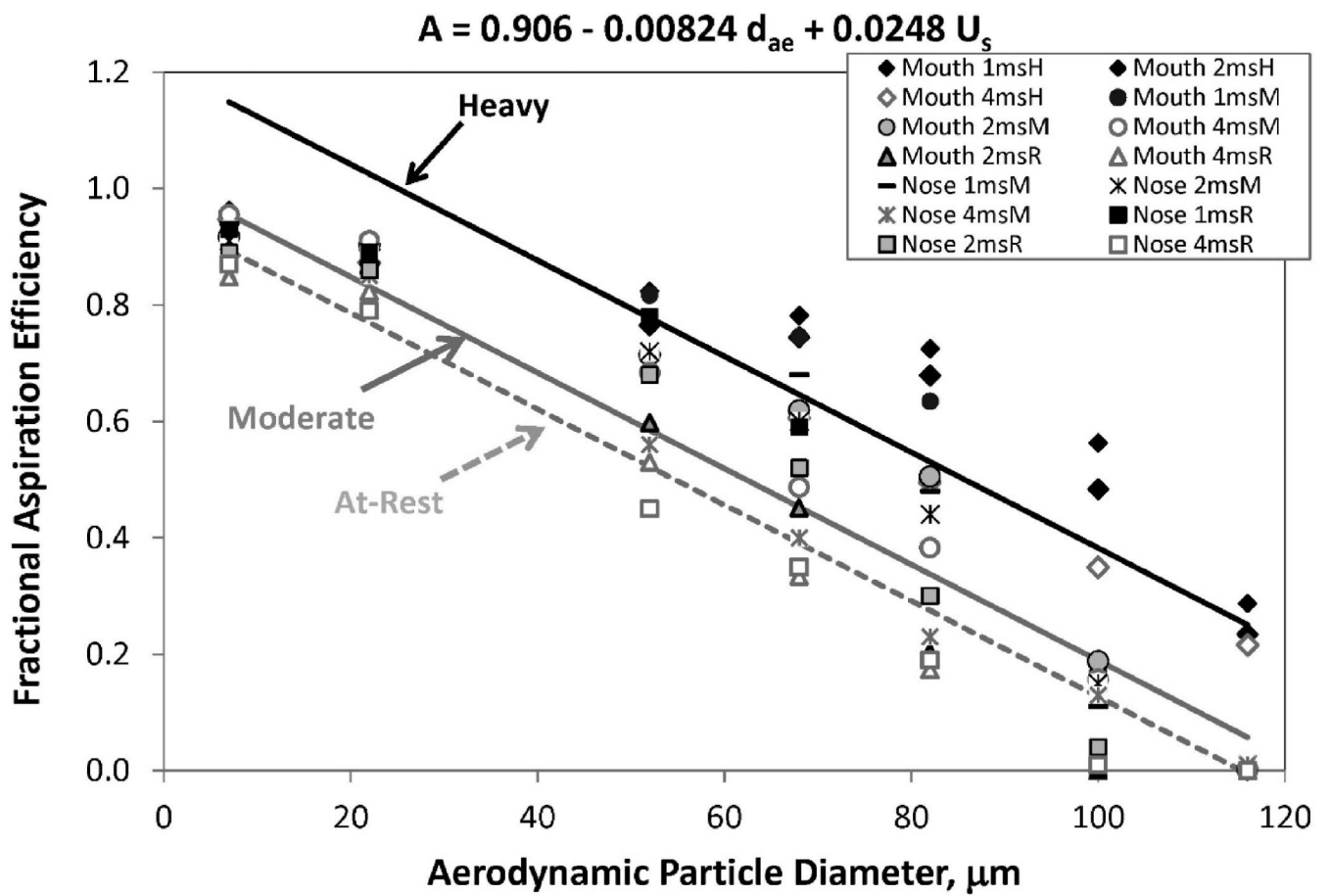


**FIGURE 4.** Empirical model ID 5 with aerodynamic diameter of particle ( $d_{ae}$ ,  $\mu\text{m}$ ) and suction velocity ( $U_s$ ,  $\text{m s}^{-1}$ ) as dependent variables ( $R^2 = 0.89$ ). Legend abbreviations indicate breathing mode (mouth or nose) followed by indication of freestream velocity (e.g., 1ms =  $0.1 \text{ m s}^{-1}$ ) followed by an indication of suction velocity (H = heavy, M = moderate, R = at-rest).

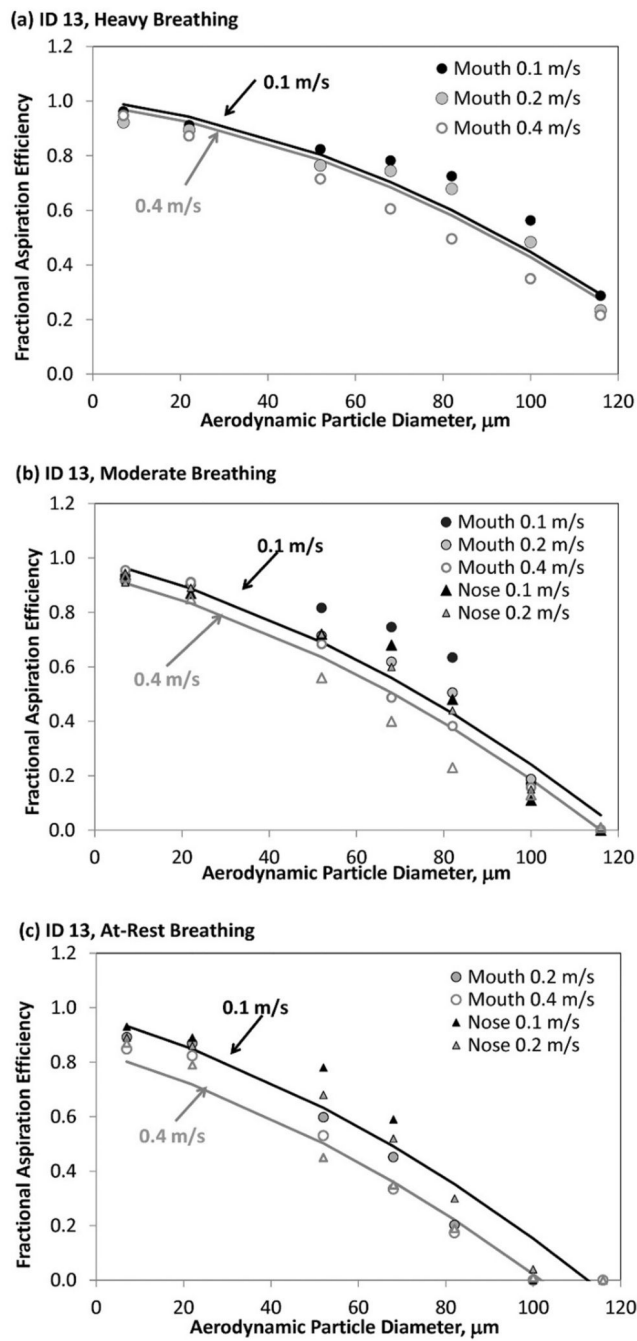


**FIGURE 5.** Empirical model ID 13 with  $d_{ae}^2$ , interaction ( $d_{ae} \times U_s$ ), and velocity ratio ( $U_o/U_s$ ) for (a) heavy, (b) moderate, and (c) at-rest breathing simulations

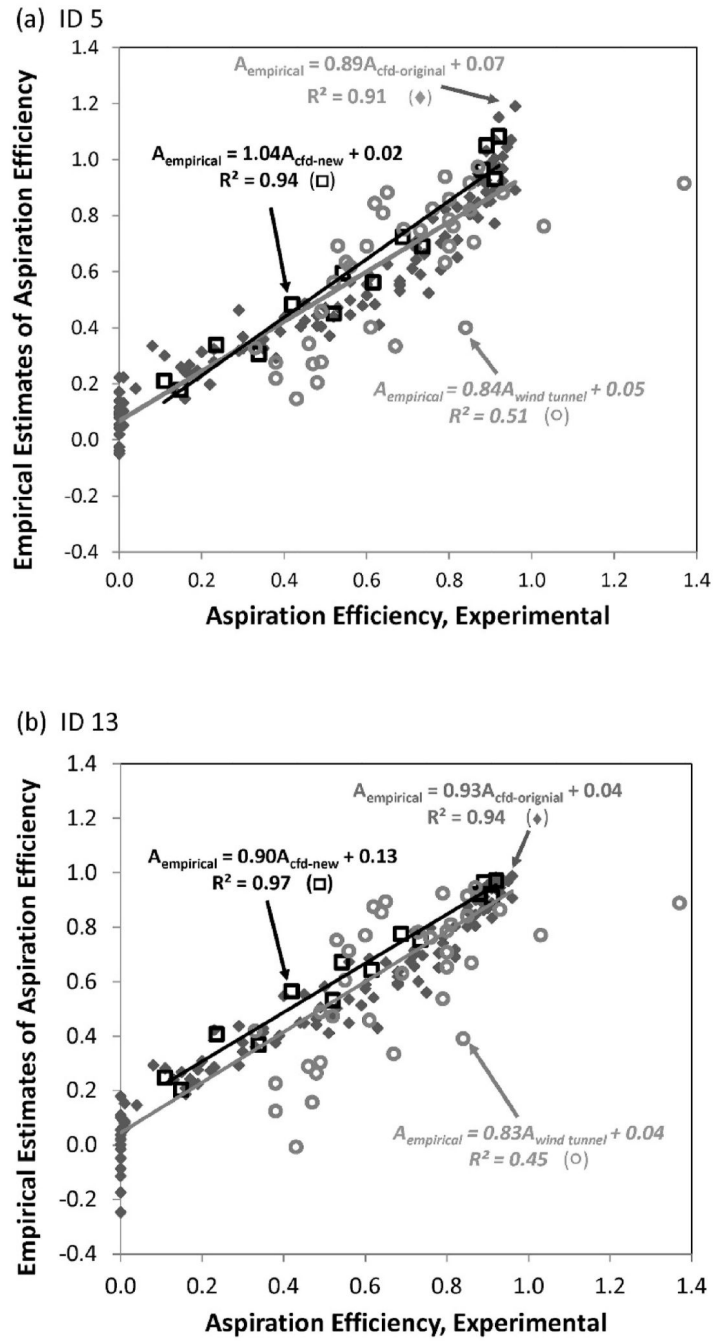


**FIGURE 6.** Comparison of experimental efficiencies to fitted empirical models using data used to generate the model (“cfd-original,” filled diamond), the new validation condition (“cfd-new,” square), and wind tunnel experimental data from Sleeth and Vincent,<sup>(12)</sup> (“wind tunnel,” round) to paired empirically estimated efficiencies using (a) linear (ID 5) and (b) second order particle size (ID 13) expressions

TABLE I

## Summary of Simulation Studies Using Female Humanoid Form

| Objective                              | Conditions   | Finding   | Reference |
|--|--|---|-----------|
| Initial study, compared to wind tunnel | Facing the wind Mouth inhalation (at-rest, moderate) Freestream velocity 0.2 and 0.4 m s <sup>-1</sup>   | Aspiration < 50% for large particles  | (15)      |
| Effect of facial feature dimensions    | Facing the wind Mouth inhalation (at-rest, moderate, heavy) Freestream velocity 0.2 and 0.4 m s <sup>-1</sup> Two nose sizes (Roman, Asian) & two lip sizes            | Efficiency ↓ by 6.5% for larger nose, 3.2% larger lips; Breathing rate accounted for 21% change               | (16)      |
| Torso simplification                   | Facing the wind Mouth inhalation (at-rest; heavy) Freestream velocity 0.1, 0.2, 0.4 m s <sup>-1</sup>  | Position of critical areas changed, but < 8.8% difference by torso shape                                      | (17)      |
| Mouth breathing *                      | Stepwise rotation (0, 15, 30, 60, 90, 135, 180°) Mouth inhalation (at-rest, moderate, heavy) Freestream velocity 0.1, 0.2, 0.4 m s <sup>-1</sup>                       | Facing-the-wind > Forward (+/-90°) > 360°; Variability in aspiration increased >22 μm                         | (19)      |
| Nose breathing *                       | Stepwise rotation (0, 15, 30, 60, 90, 135, 180°) Nose inhalation (at-rest, moderate) Freestream velocity 0.1, 0.2, 0.4 m s <sup>-1</sup> Two nose sizes (Roman, Asian) | Large nose had decreased aspiration (at matched Q); Less sensitive to breathing and freestream (5.7 and 7.2%) | (18)      |

Note:

\* Data from these setups have been incorporated into the data sets used for the empirical model development.

**TABLE II**Velocities ( $\text{m s}^{-1}$ ) Assigned to Simulation by Geometry and Breathing Mode

| <b>Breathing Rate<br/>Descriptor</b> | <b>Equivalent volumetric<br/>flow rate (<math>\text{L min}^{-1}</math>)</b> | <b>Mouth</b> | <b>Small<br/>Nose</b> | <b>Large<br/>Nose</b> |
|--------------------------------------|---|--------------|-----------------------|-----------------------|
| For empirical model generation:      |   |              |                       |                       |
| At-rest                              | 7.5   | 1.81         | 2.4                   | 1.35                  |
| Moderate                             | 18  | 4.33         | 5.74                  | 3.25                  |
| Heavy                                | 50.3  | 12.11        | —                     | —                     |
| Validation data for empirical model: |   |              |                       |                       |
| Moderate to Heavy                    | 40.2  | 9.67         | 11.09                 | —                     |

Note: Velocities were established using the mean inhalation velocity of the associated breathing rate.

**TABLE III**

Computed Omnidirectional Aspiration Fractions for Simulations at  $0.31 \text{ m s}^{-1}$  Freestream,  $40.2 \text{ L min}^{-1}$  Equivalent Inhalation Rate (New Validation Data)

| <b>dae, <math>\mu\text{m}</math></b> | <b>Mouth</b> | <b>Nose</b> |
|--------------------------------------|--------------|-------------|
| 7                                    | 0.89         | 0.92        |
| 22                                   | 0.91         | 0.88        |
| 52                                   | 0.73         | 0.69        |
| 68                                   | 0.62         | 0.54        |
| 82                                   | 0.52         | 0.42        |
| 100                                  | 0.34         | 0.24        |
| 116                                  | 0.15         | 0.11        |

Author Manuscript

Author Manuscript

Author Manuscript

Author Manuscript

**TABLE IV**

Results of Multiple Linear Regressions to Examine Associations Between Test Factors and Aspiration Fraction Estimates<sup>A</sup>

| ID  | Regression   | R <sup>2</sup> | Comments                                      |
|---|--|----------------|---|
| Simple Linear Formulation                 |  |                |   |
| 1   | $A = 1.03 - 0.00824 d_{ae}$  | 0.81           | Simplest formulation                          |
| 2   | $A = 0.904 - 0.00824 d_{ae} + 0.00602 Q$   | 0.89           | Alternative Aitken et al. <sup>(9)</sup> form |
| 3   | $A = 0.906 - 0.00824 d_{ae} + 0.0248 U_s$  | 0.89           | Alternative Aitken et al. <sup>(9)</sup> form |
| 4   | $A = 1.14 - 0.0082 d_{ae} - 0.465 U_o$   | 0.85           | Freestream velocity replaced suction velocity |
| 5   | $A = 1.008 - 0.008 d_{ae} + 0.023 U_s - 0.40 U_o$  | 0.91           | Full model with no interactions               |
| Particle Size Squared                     |  |                |   |
| 6   | $A = 0.866 - 6.6e-5 d_{ae}^2$  | 0.82           | Simplest formulation in $d_{ae}^2$            |
| 7   | $A = 0.953 - 3.5e-5 d_{ae}^2 - 0.004 d_{ae}$   | 0.83           | Adding $U_s$ yields $d_{ae}^2$ insignificant  |
| 8   | $A = 0.927 - 3.6E-5 d_{ae}^2 - 0.004 d_{ae} + 0.023 U_s - 0.405 U_o$                       | 0.93           | Backwards elimination: all in                 |
| Interactions and Dimensionless Parameters |  |                |   |
| 9   | $A = 0.885 - 4.77E-5(d_{ae}^2 \times U_o) - 0.007 d_{ae} + 0.024 U_s$                      | 0.91           | Stokes number                                 |
| 10  | $A = 0.982 - 2.53E-5(d_{ae}^2 \times U_o) - 0.0075 d_{ae} + 0.016 U_s - 0.62(U_o/U_s)$     | 0.92           | Stokes number and velocity ratio              |
| 11  | $A = 0.942 - 3.59E-5 d_{ae}^2 - 0.0039 d_{ae} + 0.014U_s - 0.83(U_o/U_s)$                  | 0.93           | Replace Stokes with $d_{ae}^2$                |
| 12  | $A = 0.953 - 2.375E-5 d_{ae}^2 - 0.004 d_{ae} - 4.6E-5 (d_{ae}^2 \times U_o)$              | 0.85           | Size and suction velocity interaction         |
| 13  | $A = 1.01 - 3.58E-5 d_{ae}^2 - 0.005 d_{ae} + 2.5E-4 (d_{ae} \times U_s) - 0.79 (U_o/U_s)$ | 0.94           | Full model with $d_{ae}^2$                    |

Note: Standard deviation of residuals, computed as (CFD-simulated aspiration efficiency) – (Empirical Model estimate of aspiration efficiency)

Particle diameter ( $d_{ae}$ ) is in  $\mu\text{m}$  and velocities ( $U_o$  and  $U_s$ ) are  $\text{m s}^{-1}$ .

TABLE V

Analysis of Residuals Associated with Models Identified in Table IV for Model Construction and for New Aspiration Estimates ( $0.3 \text{ m s}^{-1}$ ,  $40.2 \text{ L min}^{-1}$ )

| Model ID | From Data Used to Build Model (N = 112)                      |         |             |                                 | Estimated from New CFD Simulations (N = 14)                  |         |             |                                 |
|----------|--|---------|-------------|---------------------------------|--|---------|-------------|---------------------------------|
|          | Residual of Aspiration (Estimated <sub>model id</sub> – CFD) |         |             | Standard Deviation of Residuals | Residual of Aspiration (Estimated <sub>model id</sub> – CFD) |         |             | Standard Deviation of Residuals |
|          | Minimum  | Maximum | Range       |                                 | Minimum  | Maximum | Range       |                                 |
| 1        | -0.38  | 0.39    | 0.77        | 0.14                            | -0.17  | 0.08    | 0.25        | 0.07                            |
| 2        | -0.28  | 0.31    | 0.59        | 0.11                            | -0.05  | 0.20    | 0.25        | 0.07                            |
| 3        | -0.30  | 0.30    | 0.60        | 0.11                            | -0.05  | 0.20    | 0.25        | 0.08                            |
| 4        | -0.31  | 0.32    | 0.63        | 0.13                            | -0.20  | 0.05    | 0.24        | 0.07                            |
| 5        | -0.23  | 0.26    | 0.48        | 0.10                            | -0.07  | 0.16    | 0.23        | 0.08                            |
| 6        | -0.35  | 0.48    | 0.83        | 0.14                            | -0.17  | 0.02    | 0.19        | 0.06                            |
| 7        | -0.36  | 0.44    | 0.80        | 0.14                            | -0.14  | 0.03    | <b>0.17</b> | <b>0.05</b>                     |
| 8        | -0.21  | 0.28    | 0.49        | <b>0.09</b>                     | -0.07  | 0.11    | 0.18        | 0.07                            |
| 9        | -0.26  | 0.27    | 0.53        | 0.10                            | -0.08  | 0.18    | 0.26        | 0.08                            |
| 10       | -0.23  | 0.22    | 0.45        | 0.10                            | -0.07  | 0.17    | 0.24        | 0.08                            |
| 11       | -0.22  | 0.20    | <b>0.42</b> | <b>0.09</b>                     | -0.04  | 0.13    | <b>0.17</b> | 0.06                            |
| 12       | -0.30  | 0.40    | 0.71        | 0.13                            | -0.17  | 0.03    | 0.20        | 0.06                            |
| 13       | -0.25  | 0.21    | <b>0.46</b> | <b>0.08</b>                     | 0.00   | 0.17    | <b>0.17</b> | <b>0.06</b>                     |

Note: Bold values indicate best performing models.